Nuclear Engineering and Technology 55 (2023) 1559–1566

Contents lists available at ScienceDirect

Nuclear Engineering and Technology

journal homepage: www.elsevier.com/locate/net

Original Article

A 30 MeV-cyclotron-based quasi-monoenergetic neutron source

Kuo-Yuan Chu [a, d], Weng-Sheng Kuo [b], How-Ming Lee [c], Yiin-Kuen Fuh [d, *]

[a] Isotope Application Division, Institute of Nuclear Energy Research, Taiwan, ROC
[b] Nuclear Engineering Division, Institute of Nuclear Energy Research, Taiwan, ROC
[c] Physics Division, Institute of Nuclear Energy Research, Taiwan, ROC
[d] Department of Mechanical Engineering, National Central University, Taiwan, ROC

ARTICLE INFO

Article history:
Received 20 October 2022
Received in revised form
6 January 2023
Accepted 20 January 2023
Available online 14 February 2023

Keywords:
Soft error rate (SER)
Quasi-monoenergetic neutron (QMN)
Neutron target station
Cyclotron

ABSTRACT

This study developed a quasi-monoenergetic neutron source (QMN) for the semiconductor device's soft error rate test (SER). Quasi-monoenergetic neutrons are generated by $^{9}Be(p,n)^{9}B$ nuclear reaction with a 1 mm beryllium target and 30 MeV protons from a cyclotron. An 8 mm water in the back of the beryllium target is used for avoiding proton penetration. The neutron spectra simulated by MCNP showed that the peak energy was around 26.5 MeV. The heat flow and mechanical properties are numerically analyzed, and the safe operating conditions are therefore determined.

1. Introduction

Single Event Upset (SEU) is a phenomenon in which high-energy particles (such as neutrons, protons, etc.) generated by the collision of cosmic rays with atmospheric atoms interact with electronic components or their circuits, resulting in bit flips [1,2]. In recent years, due to the rapid progress of semiconductor technology, the density of components in electronic chips, memory, power transistors, and other equipment has become higher and higher, so the probability of SEU occurrence is also greater. If these electronic components are to be used in the space environment, it will become very important to implement the Soft Error Rate (SER) test.

The current international standard for soft error rate testing of electronic components is the JESD89 series [3–5]. The soft error rate test can be performed in a natural environment, but the neutron flux rate in the natural environment is low, so it takes a long time. Therefore, it is necessary to use other methods to shorten the test time. Usually electronic components need to be tested with alpha particles, fast neutrons and thermal neutrons. In the fast neutron part, the following three radiation sources can be used for simulation, which are spallation source, monoenergetic proton and quasi-monoenergetic neutron.

The Spallation sources can generate the world's strongest pulsed neutron beams for scientific research and industrial applications. However, spallation sources are large in size and complex in design. Currently, only a few countries have such facilities. This article will not discuss this application. Neutrons and protons with energy between 50 and 200 MeV have similar soft error rates, so protons can be used instead of neutrons in this energy range, but the TR-30 cyclotron used in this article has a maximum energy of 30 MeV and cannot use this method.

When the energy is between 10 and 50 MeV, the contribution of neutrons to the soft error rate is greater than that of protons, and it is not appropriate to use protons for testing. The JESD recommends the use of quasi-monoenergetic neutrons.

To study the feasibility of applying quasi-monoenergetic neutron beams to SER detection, a QMN system was established at the Institute of Nuclear Energy (INER), which is based on the TR-30 cyclotron and transmits through $^{9}Be(p,n)^{9}B$ nuclear reaction to generate neutrons, in which the proton beam energy of the nuclear reaction is 30 MeV; The maximum operable current is 9 μA, and the actual normal operation uses about 1–2 μA, In the early stage of the design of the QMN system, to understand the neutron flux rate of the beryllium target material after the nuclear reaction, the MCNP 6.2 program was used for simulation analysis. This article presents the geometric design of the QMN, the results of the Monte Carlo analysis of the sample neutron flux at different distances, the thermal analysis of the QMN system, and the solution for

* Corresponding author.
E-mail address: alextrue@iner.gov.tw (Y.-K. Fuh).

https://doi.org/10.1016/j.net.2023.01.020

measuring the proton beam current.

2. QMN system design and simulation

2.1. The neutron source system

The TR-30 cyclotron is manufactured by ACSI, Canada, and its performance information can be found in Table 1. Due to the limitation that TR-30 can only provide proton beams, the target materials for the QMN system are mainly beryllium and lithium [6,7], both of which can generate quasi-monoenergetic neutrons through (p,n) nuclear reaction, but considering the advantages of beryllium's higher melting point than lithium, lower chemical activity in the atmosphere and higher neutron yield, so this study uses beryllium metal with a purity of 99.9% as the target material [8].

The QMN system uses a beryllium metal plate with a thickness of 1 mm as the irradiation target material. The whole system includes a set of collimators, aluminum alloy beam pipes, vesple insulating plates, cooling water channels plate, and titanium foils. The aluminum alloy adopts the common Al-6061-T6 alloy. The collimator includes a set of graphite blocks (the density is 1.9 g/cm^3) for measuring the current. Refer to Fig. 1 for the system diagram.

The collimator is used to determine whether the proton beam is aligned with the center position. If the beam is deflected in a certain direction, the deflection magnet of the TR-30 cyclotron system can be used for beam correction, and The proton beam hits the beryllium target to produce a $^9Be(p,n)^9B$ nuclear reaction to produce fast neutrons. When the QMN system produces quasi-monoenergetic neutrons, it will be accompanied by protons. In order to avoid the mixed impact of neutrons and protons on the sample, it is necessary to block the protons, so as to evaluate the test effect of SER.

Consider using water as a shield for the protons, as water works well for blocking protons and at the same time cools the beryllium target as shown in Fig. 1. To know the thickness of the water shield, the SRIM program can be used to first calculate the energy protons in the beryllium target. The average range (Projected Range) [9], and then interpolate to find the proton energy E_f after passing through the beryllium target, and finally use the SRIM program to calculate the average range of protons with this energy walking in the water to determine the appropriate water shielding thickness.

Referring to the average range data in Table 2, the range difference between 30 MeV and 27.5 MeV is

$$\Delta S = 0.85\ (\mathrm{mm})$$

Since ΔS is less than 1 mm, it can be known that the energy E_f of the proton after passing through the beryllium target will be between 27.5 and 25 MeV, and the interpolation method is used here:

$$\frac{(27.5-25)}{0.78} = \frac{\left(27.5-E_f\right)}{(1-0.85)} \Rightarrow E_f = 27.02\ (MeV)$$

The SRIM program again calculated that the average range of protons with energy E_f traveling in water is 7.21 mm, and finally chose to use a water shield thickness of 8 mm. The influence of gamma rays produced in the process of generating neutrons by SER irradiation work is not discussed in this paper, which requires more experiments in the future.

Table 1
TR-30 cyclotron parameters.

Basic performance parameters	
Partical	H-
Energy(MeV)	15–30
Maximum proton intensity(μA)	1000
Simultaneous extracted beams	2
Ion source	
Type of ion source	External multicusp
Vacuum system	Cryo & Turbo pump
RF system	
Frequency (MHz)	73.129
Power amp.(kW)	100
Dee voltage (kV)	50
Harmonic mode (proton)	4
Miscellaneous parameters	
Main magnet sectors	4
Beam exit ports	13

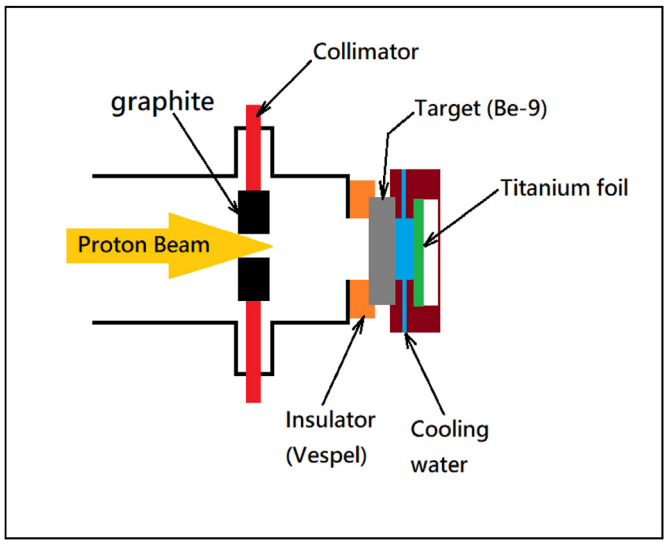

Fig. 1. QMN system schematic diagram.

2.2. Monte-carlo simulation

In the study of Kim et al., a proton beam of 35 MeV was used to bombard a beryllium target with a thickness of 0.5 mm. As a result, the neutron peak energy was about 33.4 MeV and its half maximum width was about 1.7 MeV [10]. The research of Kamata et al. focused on the quasi-monoenergetic neutron effect at a specific angle, and found that when the angle between the target position and the proton beam exceeds a certain angle, the quasi-monoenergetic effect will be affected. This angle is 30° for the lithium target and 16° for the beryllium target. Both materials have the best effect at 0°, and the beryllium target is more sensitive to angle changes than lithium [11].

The study by Novák et al. compared the difference between lithium and beryllium for the production of quasi-monoenergetic neutrons. The thickness of the beryllium target was 0.5 mm and the thickness of the lithium target was 2 mm. Before actually measuring the neutron energy spectrum, the team first used MCNPX The program performs the simulation, and the results can be referred to Fig. 2 [12].

It can be roughly judged from Fig. 2 that the beryllium target has about 5 peaks, and the lithium target has 2 peaks. Comparing the characteristics of producing quasi-monoenergetic neutrons, lithium is better than beryllium. In terms of neutron yield, there is not much difference between the two, but if only look at the 20–30 MeV range, the beryllium target will be larger than the lithium. Because the melting point of beryllium is much higher than that of lithium, the beryllium target can withstand higher irradiation current, and its target station operation performance will be better than lithium.

Table 2
The average range of protons in beryllium is calculated by SRIM.

Ion Energy (MeV)	dE/dx Elec. (MeV/mm)	dE/dx Nuclear (MeV/mm)	Projected Range (mm)	Longitudinal Straggling (μm)	Lateral Straggling (μm)
15	5.02E+00	2.09E-03	1.66	66.1	36.4
16	4.76E+00	1.97E-03	1.86	72.47	40.76
17	4.53E+00	1.86E-03	2.07	78.95	45.33
18	4.32E+00	1.77E-03	2.3	85.53	50.12
20	3.97E+00	1.61E-03	2.78	110.12	60.32
22.5	3.60E+00	1.44E-03	3.44	145.3	74.22
25	3.31E+00	1.31E-03	4.17	178.67	89.37
27	3.06E+00	1.20E-03	4.95	211.4	105.74
30	2.85E+00	1.11E-03	5.8	244.02	123.3

The energy spectrum has a tail at low energy range which is similar to the simulation results in this study. The tailing might account for a given percentage of SERs. For example, with the energy-dependent SER cross section for a 40-nm FPGA as reported by Ref. [13], the monoenergetic peak and the peak below should cause about 55% and 45% of expected SERs, respectively. Although the QMN source has not a perfect spectrum to SER test, it could be a handy tool for prescreening of SERs. Frankly speaking, the spectrum of our neutron source is better regarded as QMN-like spectrum.

Based on the above conclusions, beryllium with a thickness of 1 mm was used as the target material in this study. The physical model used in the simulation is shown in Fig. 3 and the simulation parameters include proton energy 30 MeV, proton current 1 μA, and incident angle 0°. The simulation results of the quasi-monoenergetic neutron spectrum are shown in Fig. 4 including the neutron spectrum at three positions, which are respectively 3, 5, and 10 cm from the back of the beryllium target; The lower the distance, the more consistent with the theory and expectations.

Looking at Fig. 4, the neutron spectrum can be roughly divided into three blocks: >22 MeV, 10–22 MeV, and <10 MeV. The most important and most concerned is the block >22 MeV, this block is where the quasi-monoenergetic neutrons are located, there is a broad peak between 22 and 28 MeV, and about 26 MeV in the middle. There is a sharper main peak of maximum energy near 2 MeV. Generally, the main peak energy of quasi-monoenergetic is about 2 MeV lower than the incident proton energy. The main peak of the developed QMN has a peak width of about 4 MeV, which should be related to the thicker beryllium target (see Table 3).

In the 10–22 MeV block, there is a relatively obvious peak at 19 MeV, but the peak height is much lower than the main peak at 26 MeV. When the neutron energy is from 22 MeV to 10 MeV, the neutron flux rate shows a gradual increase trend, which is speculated that the higher energy neutrons are slowed down when penetrating the target.

In the <10 MeV block, two distinct peaks can be found, the highest peak occurs at about 2 MeV, and the secondary peak occurs at about 6 MeV, and the flux rate of 2 MeV is even higher than that of the main peak of maximum energy. Fortunately, for particles with energy in this region, the probability of a single event upset (SEU) is much lower than that of particles above 10 MeV.

Table 4 summarizes the neutrons flux rates for the interval of interest and defines their lower energy bounds here. If 22 MeV is taken as the lower limit of the neutron energy, they will account for 32%–34%; if we only look at the 25 MeV part, they will only account for 19%–23%.

As far as the ideal neutron flux rate ($\geq 10^8$ n·cm^{-2}·s^{-1}) is concerned, when 22 MeV is used as the lower limit of the quasi-monoenergetic value, the position 5 cm behind the beryllium target (neutron flux rate 1.04 × 10^8 n·cm^{-2}·s^{-1}) can meet expectations.

2.3. Analysis of stress and heat transfer in the QMN system

To understand the reliability of the mechanical design of the quasi-monoenergetic neutron target, simulations were conducted with COMSOL Multiphysics® v5.5 [14]. The three-dimensional physical model is shown in Fig. 5.

The simulation uses three COMSOL modules: the basic module, the heat transfer module, and the fluid mechanic module. The fluid

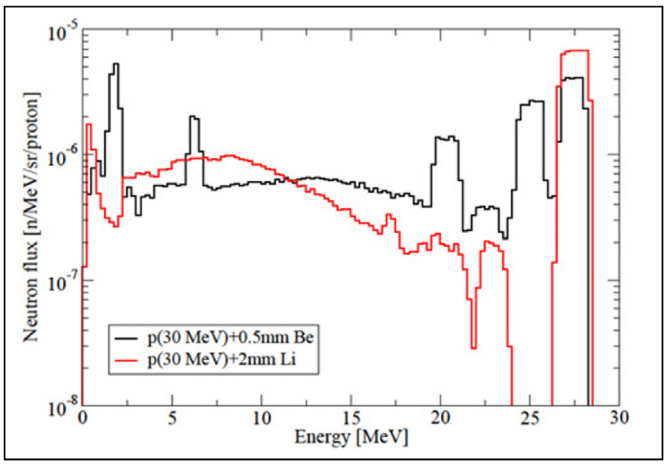

Fig. 2. MCNPX (ENDFB-VII and LA 150 libraries were used) simulated neutron spectra from the reactions p + Be and p + Li with 30 MeV protons [12].

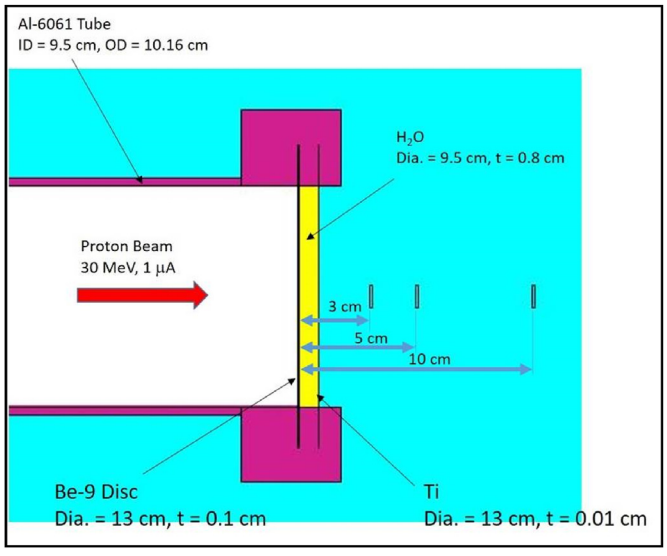

Fig. 3. Physical model for MCNP simulation.

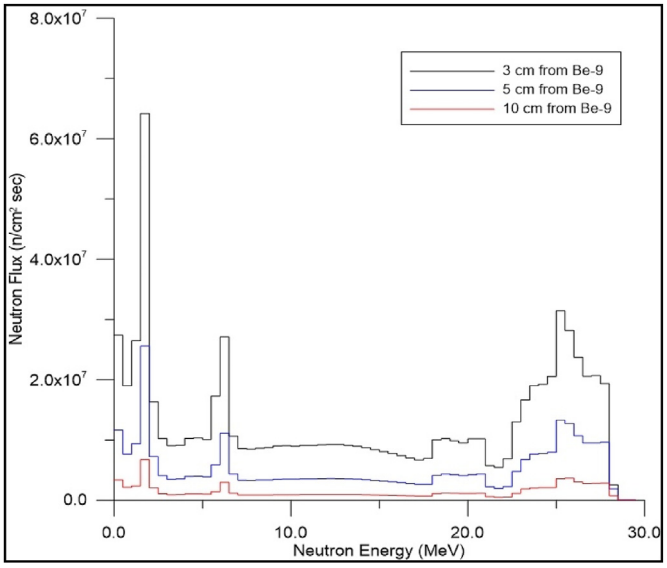

Fig. 4. MCNP 6.2 simulation results – quasi-monoenergetic neutron spectrum.

mechanic module solves the flow problem of cooling water, the heat transfer module the heat transfer problem, and the basic module the mechanical stress. The thermal expansion problem is estimated by the analytical equation of the basic module. To improve the convergence of numerical solutions, the numerical problem is solved by two steps: the flow field equations are solved in advance, and then all equations are solved fully coupled with the previously obtained results as initial conditions.

The heat source on the neutron target is a proton beam of 30 MeV, 10 μA, and FWHM = 1 cm. Since a thin Beryllium target is used, most of irradiated protons penetrate the target. Although the heat distribution in the target system is a volumetric distribution in real case, the simulation of this study were conducted with two surface heat sources, i.e., one on the beryllium target and the other in the cooling water. A surface heat source on the beryllium target was set on the beryllium surface at the incident proton side. A surface heat source in the cooling water was set at the position of the proton range in the cooling water. The heat distribution on the two heat source surfaces were of FWHM of 1 cm. Above simulation conditions can be regarded as a worse case for heat transfer, so the neutron target system should be operating safe once it passes the above extreme conditions.

The simulation results are summarized in Figs. 6–10. Fig. 6 shows the flow velocity distribution and streamline of the neutron target cooling water. The boundary conditions of the simulated cooling water inlet are velocity 0.1 m/s, and temperature 25 °C. To avoid the potential risk of air bubbles accumulating, cooling water enters from the lower two ducts and flows out from the upper two ducts. From the simulation results, it can be seen that there is a short flow, the cooling water mostly flows out from the lower inlet to the upper outlet, and there is an obvious backflow situation on the left and right sides of the water channel interlayer. As a result, a clear temperature distribution is formed. The position with the highest thermal deposition in the center has a relatively low temperature, while the temperature in the reflow zones on both sides is higher due to poor convection. However, on the whole,

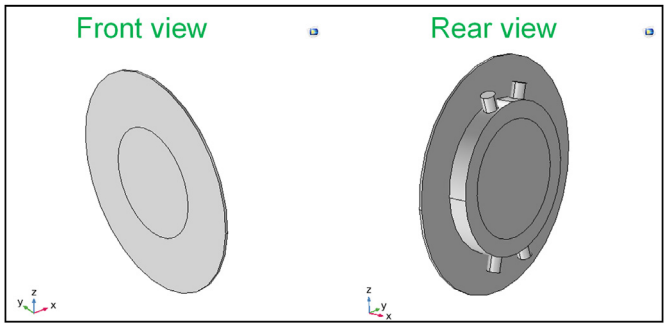

Fig. 5. Comsol physical model for mechanical stress analysis of QMN

Table 3
Beryllium Target Thickness vs. Stopping Distance for Quasi-monoenergetic Neutron Sources.

literature	Proton Beam Energy (MeV)	Beryllium target thickness (mm)	stopping distance (mm)	Beryllium target thickness/stopping distance
[10]	35	0.5	7.67	0.065
[11]	70	3.0	26.85	0.112
[12]	30	0.5	5.80	0.086
This article	30	1.0	5.80	0.172

Table 4
Quasi-monoenergetic neutron flux $n \cdot cm^{-2} \cdot s^{-1}$ and its proportion..

With target window distance / Neutron energy range	3 cm	5 cm	10 cm
≥10 MeV	7.67×10^8 (100%)	3.31×10^8 (100%)	8.47×10^7 (100%)
≥22 MeV	2.42×10^8 (32%)	1.04×10^8 (33%)	2.91×10^7 (34%)
≥25 MeV	1.15×10^8 (19%)	5.40×10^7 (22%)	1.58×10^7 (23%)

the maximum temperature of 65 °C is much lower than the boiling point of water, which is a safe and operable range. Therefore, in actual operation, as long as the temperature of the inflow cooling water is controlled to be around 25 °C, the operation should be safe.

Fig. 7 shows the temperature distribution of the beryllium target. The highest temperature in front of the beryllium target (proton incident surface) is 88.7 °C, which is much lower than the melting point of beryllium. The thermal melting problem of the beryllium target should not be a problem. However, the radial temperature difference on the surface of the beryllium target is about 30 °C. Whether there will be thermal expansion deformation and stress problems will be further clarified in the subsequent mechanical stress analysis.

The analysis results of mechanical stress are organized in Figs. 8–10. This study focuses on three kinds of stress in the analysis: (1) von Mises stress: the reference standard criterion for stress tensor calculation. (2) Yield strength: also known as yield stress or strength and toughness. The definition in mechanical and material science is the elastic limit of ductile materials under stress. After exceeding this strength, an unrecovered deformation may occur. (3) Ultimate tensile strength: the stress value of the material when it breaks during the tensile process. To facilitate interpretation, this study uses the following two ratios to judge the results:

$$R_1 = (\text{von Mises stress})/(\text{yield strength}) \quad (1)$$

$$R_2 = (\text{von Mises stress})/(\text{ultimate tensile strength}) \quad (2)$$

Among them, $R_1 \geq 1.0$ means that the yield strength is exceeded, and the material may undergo irreversible permanent deformation, but it may not rupture. $R_2 \geq 1.0$ indicates that the ultimate tensile strength is exceeded and the material has ruptured. Based on the safety of material handling, R1 should be less than 1.0, and R2 should never exceed 1.0.

Fig. 7 shows the effect of cooling water pressure on yield strength and deformation displacement. The cooling water includes 4 pressures of 0, 1, 2, and 3 bar. The 0 bar condition is a practically impossible physical condition. This condition is used to understand the effect of thermal expansion, because there is no pressure difference between the two ends of the beryllium target, and all the stress of the beryllium target comes from thermal expansion. The 1 bar condition is the minimum pressure for practical operation because the cooling water pressure is equal to atmospheric pressure plus head pressure and mechanical delivery pressure. The 2 and 3 bar conditions were used as controls.

Fig. 8 shows the R1 ratio (von Mises stress/yield strength) of the tangent lines in the y and z directions on the front and rear sides of the beryllium target. It can be easily interpreted from the figure. Under the three conditions of water pressure 0, 1, and 2 bar, R1 is less than 1.0; When the water pressure is 3 bar, part of the central area and edge of the beryllium target are greater than 1.0. In short, the cooling water pressure should be controlled below 2 bar, which is a relatively safe operating condition.

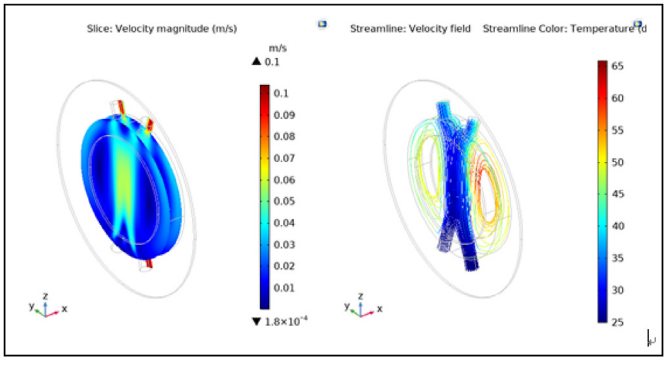

Fig. 6. Velocity distribution (left) and streamline (right) of cooling water at neutron target station (Boundary conditions for cooling water inlet: velocity 0.1 m/s, temperature 25 °C.).

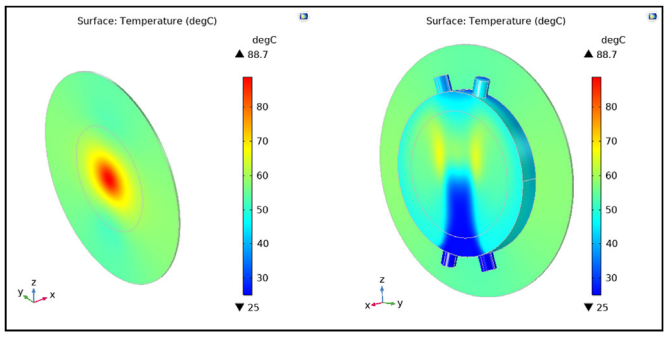

Fig. 7. Temperature distribution in front (left) and behind (right) of the neutron target station (Heat source parameters: 30 MeV, 10 μA, FWHM = 1 cm).

Fig. 9 shows the R2 ratio (von Mises stress \ Ultimate tensile strength) of different tangents of the beryllium target. Under all the hydraulic pressure conditions of this simulation, R2 is all less than 1.0, indicating that the beryllium target will not be broken during operation. The above results are acceptable because once the beryllium target breaks, the cooling water will enter the proton beam tube, which may pose a threat to the front-end vacuum pump and even the cyclotron.

3. Relationship between the proton current and the Be target current

A thinner beryllium target is the required part for quasi-monoenergetic neutron production. After the nuclear reaction is over, the protons will pass through the beryllium target and lose some energy. The cooling water behind the beryllium target will further decelerate the protons, and finally stop in the water. However, if the cooling water circulation line is grounded, the measured irradiance current will be incorrect. To solve this problem, we planned two experiments. Experiment 1 assumes that after the proton beam passes through the beryllium target, some residual current can still be measured in the beryllium target, and the main current disappears in the cooling water and cannot be measured. We want to know whether there is a linear relationship between the residual and the main current. If we know its linear equation, we can use it to infer the main current during irradiation. During this experiment, cooling water is temporarily not supplied to allow protons to penetrate the beryllium. After the target, the Faraday cup at the beam outlet was used to measure the main current, and the two currents were recorded separately for the current graph drawing.

Experiment 2 is to insulate the pipeline through which the cooling water flows to know whether the complete output current can be directly measured. For this purpose, we use a peristaltic pump drive for the cooling water circulation. All waterway parts including water pipes, T-joints, and cooling water collection bottles are made of insulating materials such as plastic or glass. Since the pipes are well insulated and the peristaltic pump is not in direct contact with the cooling water the current is not grounded.

The two experimental plans described above can be referred to as shown in Figs. 11 and 12. Because of the need to observe whether the proton beam cannot penetrate the cooling water shield, the

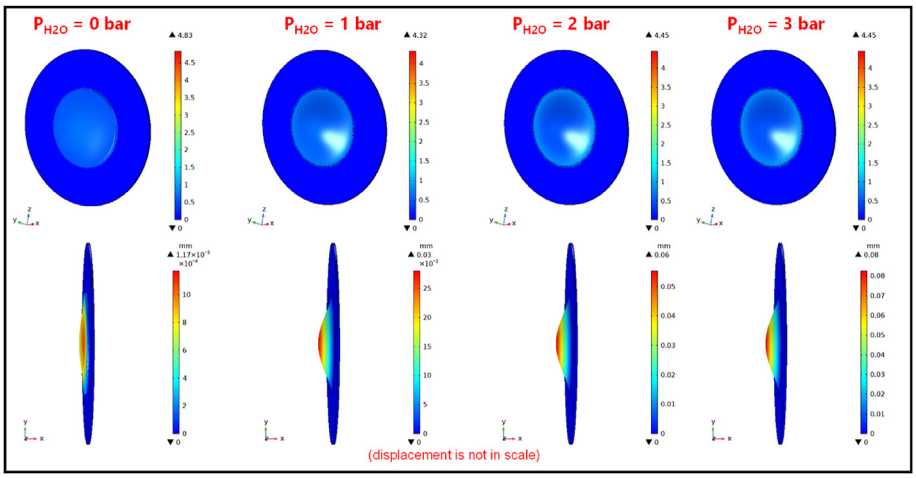

Fig. 8. Effects of cooling water pressure on yield strength (top) and deformation displacement (bottom) (The value in the upper graph is the ratio of von Mises stress to the yield strength of the material. The value in the lower graph is the displacement.).

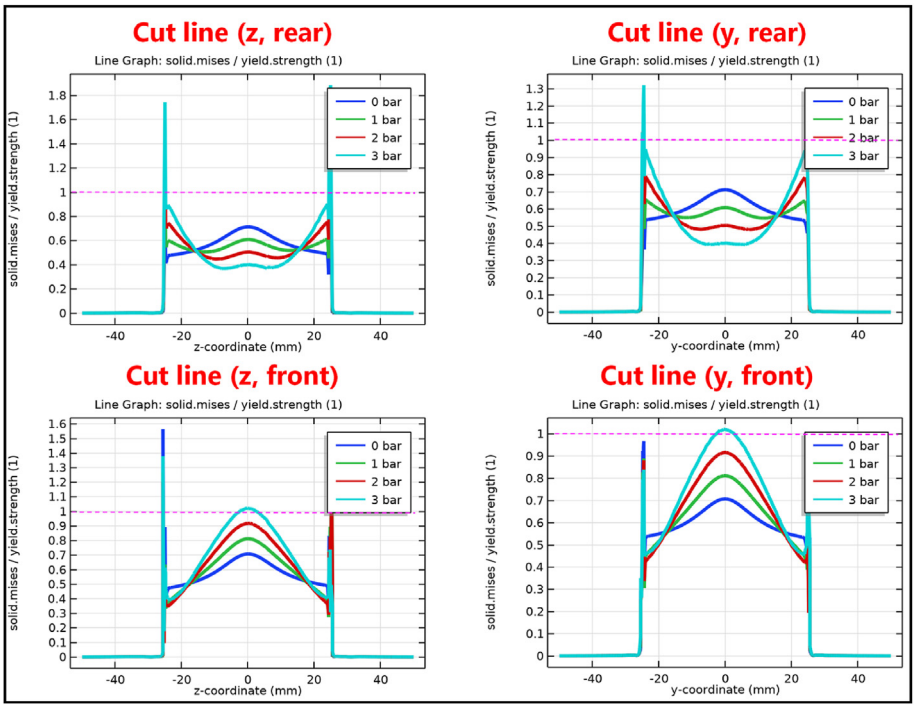

Fig. 9. The ratio of von Mises stress to material yield strength at different tangents for beryllium targets.

Faraday cup is still retained in experiment 2.

3.1. Experiments without cooling water

Experiment 1 was carried out according to the experimental plan. First of all, we need to prepare the experimental equipment in advance, including the QMN system, Faraday cup, precision ammeter, and standard current source. The design of the Faraday cup considers the secondary electron recovery mechanism to reduce measurement errors; the ammeter is calibrated by the instrument supplier before leaving the factory, and the standard current source has been calibrated before the experiment is carried out.

All signal lines related to current measurement work must be included in the pre-experiment calibration work to ensure that the current measurement value is credible. We connect the current source to the Faraday cup signal line and input a 1 μA test signal. As a result, we get a current value of 0.999 μA on the ammeter, and the current value error is less than one thousandth, so we think such an error value is acceptable. The same test procedure is also implemented for the signal line used for the beryllium target, and the result shows a readback value of 0.999 μA on the ammeter.

The placement of the equipment in experiment 1 is the same as the plan in Fig. 11. After the experiment, it is confirmed that a small residual current can be measured on the beryllium target and the main current can be measured on the Faraday cup. There is a linear

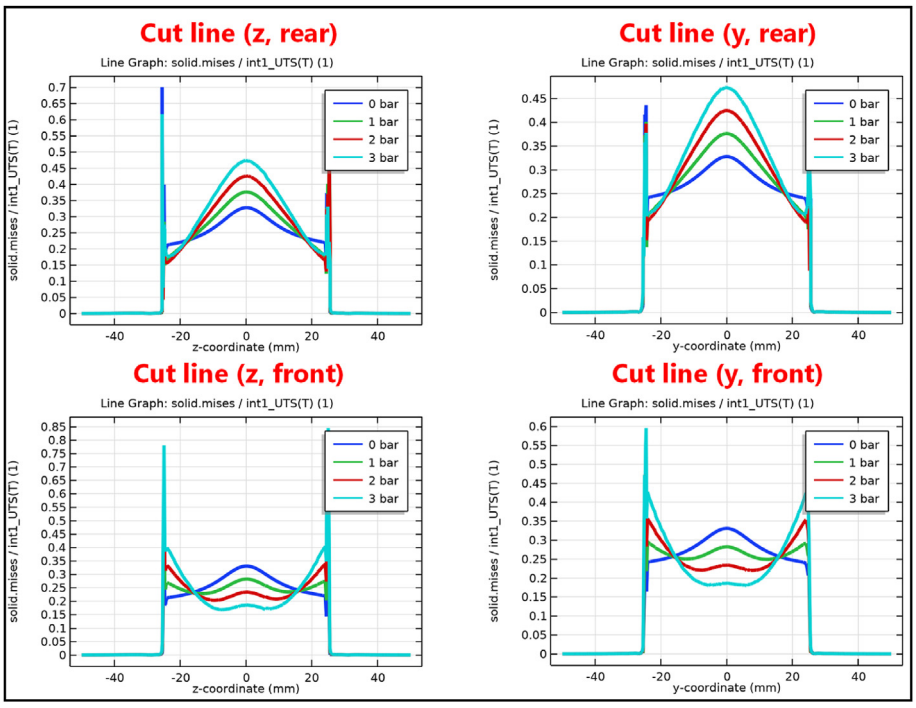

Fig. 10. The ratio of von Mises yield strength to ultimate tensile strength at different tangents to beryllium targets.

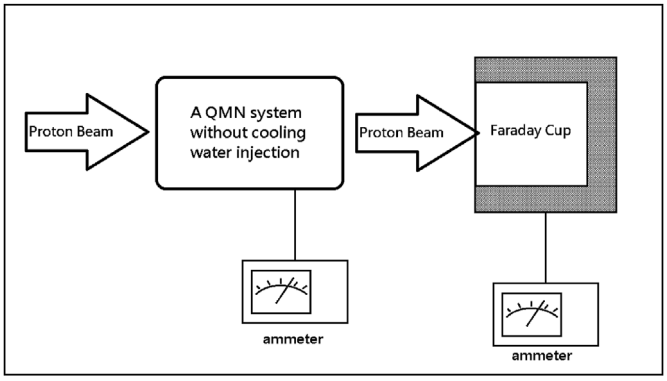

Fig. 11. Schematic diagram of experiment 1.

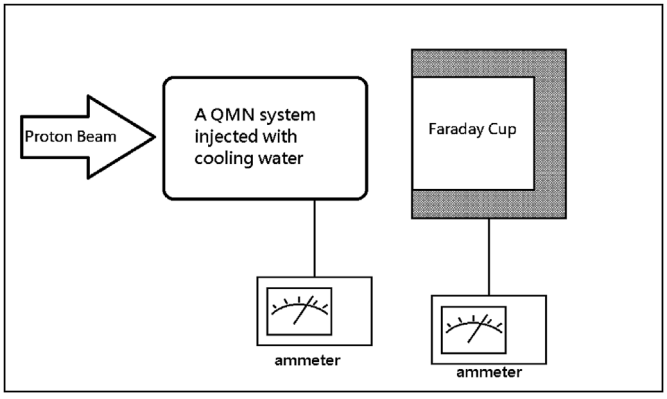

Fig. 12. Schematic diagram of experiment 2.

relationship between the two. The relevant experimental data can refer in Table 5; the relationship between the Faraday cup and the beryllium target current can be referred in Fig. 13.

The EPR current in Table 5 is the current value when the proton beam is extracted inside the TR-30 accelerator. It is measured by the interface card of the accelerator system, but since the interface card has not been calibrated, the measured value can only be used as a reference. The measured data is shown in Fig. 12 and the graph was linearized using EXCEL. We can observe that the actual beryllium target to Faraday cup current correspondence fits the equation well with the straight line.

The placement of the equipment in Experiment 1 is the same as the plan in Fig. 10. After the experiment, it is confirmed that a small residual current can be measured on the beryllium target and the main current can be measured on the Faraday cup. There is a linear relationship between the two. The relevant experimental data can refer to in Table 3; the relationship between the Faraday cup and the beryllium target current can be referred to in Fig. 12.

The EPR current in Table 5 is the current value when the proton beam is extracted inside the TR-30 accelerator. It is measured by the interface card of the accelerator system, but since the interface card

Table 5
Measurement data for Experiment 1.

EPR current (nA)	Be Target (nA)	Faraday Cup Current (nA)
57	2.4	20
238	15.14	100
730	42.96	300
1200	68.6	500
1710	94.4	715
2440	136.24	1000
3660	193.6	1500

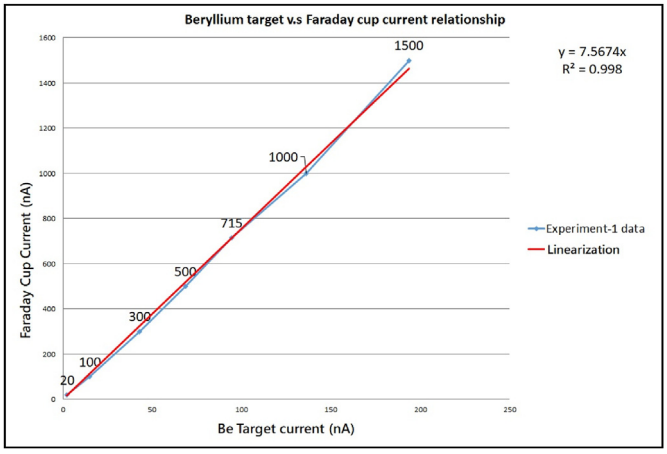

Fig. 13. The relationship between beryllium target and Faraday cup current.

Table 6
Measurement data for Experiment 2.

EPR Current (nA)	Faraday Cup current (nA)	Be Target (nA)
730	550	540
1950	1170	1280
3170	2008	2190

has not been calibrated, the measured value can only be used as a reference. The measured data is shown in Fig. 12 and the graph was linearized using EXCEL. We can observe that the actual beryllium target to Faraday cup current correspondence fits the equation well with the straight line.

3.2. Experiments with cooling water

Experiment 2 needs to provide cooling water to the QMN system. The key point of observation is whether the cooling water can really shield the proton beam. This can be determined by whether the Faraday cup produces current. In addition, it was tested whether the full current could be measured directly from the beryllium target. Finally, perform a durability test on the QMN system, use a proton current of 2 μA for 30 min and observe whether the current can be measured on the Faraday cup. If the current can be measured, it means that the cooling water has generated bubbles so that the protons can penetrate the cooling water shielding, the cooling system performance had to be improved to avoid this situation, luckily none of these things happened till the end of the test, the system worked smoothly as expected.

The data for Experiment 2 can be found in Table 6. Before the experiment, measure the output current through the Faraday cup and record the corresponding EPR current. In this way, after the cooling water is supplied to the QMN system, we can still judge whether the input proton beam current is sufficient according to the EPR current.

4. Conclusion

A QMN or QMN-like neutron source has been successfully developed, simulated, and constructed in this study. Based on MCNP simulation results, the neutron spectra showed a peak energy at around 26.5 MeV, as well as some peaks at lower energy range. The mechanical design is safe with numerical analysis and experimental verification. Experimental results showed that the incident proton current can be directly and correctly measured at the beryllium target without the aid of other equipment. The neutron spectrum shown in this paper is based on MCNP simulation, further study on experimental measurement is deemed necessary. Authors are planning to measure fast neutron spectrum with a Bonner sphere spectrometer and TOF technique, and hope to provide the experimental data soon in the coming future. Overall speaking, the new QMN or QMN-like neuron source proposed in this study could be a handy tool for the SER test.

Declaration of competing interest

The authors declare that they have no known competing financial interests or personal relationships that could have appeared to influence the work reported in this paper.

References

[1] T.J. O'Gorman, et al., Field testing for cosmic ray soft errors in semiconductor memories, in: IBM Journal of Research and Development, vol. 40, 1996, pp. 41–50.
[2] A. Lesea, et al., The rosetta experiment: atmospheric soft error rate testing in differing technology FPGAs, in: IEEE Transactions on Device and Materials Reliability, vol. 5, 2005, pp. 317–328.
[3] JEDEC® Standard JESD89, Measurement and Reporting of Alpha Particles and Terrestrial Cosmic Ray-Induced Soft Errors in Semiconductor Devices, JEDEC® Solid State Technology Association, 2001.
[4] JEDEC® Standard JESD89A, Measurement and Reporting of Alpha Particle and Terrestrial Cosmic Ray Induced Soft Errors in Semiconductor Devices, JEDEC® Solid State Technology Association, 2006.
[5] JEDEC® Standard JESD89B, Measurement and Reporting of Alpha Particle and Terrestrial Cosmic Ray Induced Soft Errors in Semiconductor Devices, JEDEC® Solid State Technology Association, 2021.
[6] D.T.L. Jones, Monoenergetic neutron sources below 100 MeV, Radiat. Phys. Chem. 61 (2001) 469–472.
[7] Zdeněk Matěj, et al., The methodology for validation of cross sections in quasi monoenergetic neutron field, Nucl. Instrum. Methods Phys. Res. A 1040 (2022), 167075.
[8] Vivek Chavan, et al., Monoenergetic neutrons from the ^{9}Be(p,n)^{9}B reaction induced by 35, 40 and 45-MeV protons, Nucl. Phys. 1018 (2022), 122374.
[9] James F. Ziegler, et al., Srim – the stopping and range of ions in matter, Nucl. Instrum. Methods Phys. Res. B 268 (2010) 1818–1823, 2010.
[10] J.H. Kim, et al., A measurement of monoenergetic neutrons from ^{9}Be(p,n)^{9}B, J. Kor. Phys. Soc. 32 (1998) 462–467.
[11] S. Kamata, et al., Tail correction in quasi-monoenergetic neutron source, CYRIC Annual Report 2005 (2005) 31–33.
[12] J. Novák, et al., The p + ^{9}Be (thin target) reaction as a source of quasi-monoenergetic neutrons, EPJ Web Conf. 146 (2017), 03013, https://doi.org/10.1051/epjconf/201714603013. ND2016.
[13] H. Iwashita, et al., Energy-resolved soft-error rate measurements for 1–800 MeV neutrons by the time-of-flight technique at LANSCE, IEEE Trans. Nucl. Sci. 67 (2020).
[14] COMSOL® Multiphysics v.5.5. https://www.comsol.com/. (Accessed 26 August 2022).